JGR Oceans

RESEARCH ARTICLE
10.1029/2023JC020117

Key Points:

- We used 13 on-iceberg GPS units to constrain upper-layer (0–250 m) circulation in Ilulissat Icefjord, west Greenland
- Deviations in down-fjord iceberg trajectory coincide with tributary meltwater flux, in both location and timing
- The speed of upper-layer circulation changes in concert with glacier behavior, including glacier speed and meltwater runoff

Supporting Information:

Supporting Information may be found in the online version of this article.

Correspondence to:

S. J. N. Baratta,
sydney.baratta@maine.edu

Citation:

Baratta, S. J. N., Schild, K. M., & Sutherland, D. A. (2024). Ilulissat Icefjord upper-layer circulation patterns revealed through GPS-tracked icebergs. *Journal of Geophysical Research: Oceans*, *129*, e2023JC020117. https://doi.org/10.1029/2023JC020117

Received 7 JUN 2023
Accepted 19 NOV 2023

Ilulissat Icefjord Upper-Layer Circulation Patterns Revealed Through GPS-Tracked Icebergs

Sydney J. N. Baratta[1,2], Kristin M. Schild[1,2], and David A. Sutherland[3]

[1]School of Earth and Climate Sciences, University of Maine, Orono, ME, USA, [2]Climate Change Institute, University of Maine, Orono, ME, USA, [3]Department of Earth Sciences, University of Oregon, Eugene, OR, USA

Abstract The Greenland Ice Sheet has undergone rapid mass loss over the last four decades, primarily through solid and liquid discharge at marine-terminating outlet glaciers. The acceleration of these glaciers is in part due to the increase in temperature of ocean water in contact with the glacier terminus. However, quantifying heat transport to the glacier through fjord circulation can be challenging due to iceberg abundance, which threatens instrument survival and fjord accessibility. Here we utilize iceberg movement to infer upper-layer fjord circulation, as freely floating icebergs (i.e., outside the mélange region) behave as natural drifters. In the summers of 2014 and 2019, we deployed transmitting GPS units on a total of 13 icebergs in Ilulissat Icefjord, an iceberg-rich and historically data-poor fjord in west Greenland, to quantify circulation over the upper 0–250 m of the water column. We find that the direction of upper-layer fjord circulation is strongly impacted by the timing of tributary meltwater runoff, while the speed of this circulation changes in concert with glacier behavior, which includes increases and decreases in glacier speed and meltwater runoff. During periods of increased meltwater runoff entering from tributary fjords, icebergs at these confluences deviated from their down-fjord trajectory, even reversing up-fjord, until the runoff pulse subsided days later. This study demonstrates the utility of iceberg monitoring to constrain upper-layer fjord circulation, and highlights the importance of including tributary fjords in predictive models of heat transport and fjord circulation.

Plain Language Summary The Greenland Ice Sheet has been rapidly losing mass over the last four decades, primarily at its edges through glacier melting and iceberg calving into fjords. Warming ocean water in contact with the glacier terminus can accelerate mass loss. However, quantifying the currents that transport this warm ocean water are challenging to constrain due to the abundance of icebergs in the near-terminus region. Here, we track freely floating icebergs, natural drifters, to infer surface circulation (0–250 m depth) in an iceberg-rich fjord. In the summers of 2014 and 2019, we deployed GPS units on 13 icebergs in Ilulissat Icefjord, a historically data-poor fjord in west Greenland. We find the direction of currents to be strongly impacted by tributary fjord runoff, with changes in iceberg trajectory coinciding with runoff pulses from these tributary fjords. We find the circulation speed to be most closely associated with glacier speed and meltwater runoff from the glacier at the head of Ilulissat Icefjord. This study highlights the utility of using icebergs to infer surface circulation and the importance of including tributary fjords in future circulation models.

1. Introduction

The Greenland Ice Sheet (GrIS) has undergone a six-fold acceleration in mass loss over the last four decades (Mouginot et al., 2019), reaching a peak (melt season maximum) mass loss rate of 200 ± 12 Gt yr^{-1} (2003–2019), contributing ~8.9 mm to total sea level equivalent (Smith et al., 2020). The increase in mass loss has been attributed to both climate and ocean warming at tidewater glacier margins, as their low elevations and direct contact with water makes them particularly sensitive to increases in temperature (Gladish et al., 2015; Slater & Straneo, 2022; Wood et al., 2021). Jakobshavn Isbræ (here after referred to by its Greenlandic name, Sermeq Kujalleq) has been the largest single contributor to GrIS mass loss since 2000 (Mouginot et al., 2019), and has undergone a series of dramatic changes, including a 15 km retreat of its floating ice tongue between 1991 and 2006, before pinning to the present-day location. Warming shelf water has been implicated in the changes observed at Sermeq Kujalleq (ice tongue retreat, glacier acceleration, increases in calving; e.g., Gladish et al., 2015; Holland et al., 2008; Joughin et al., 2020; Khazendar et al., 2019; Motyka et al., 2011), as the transport of warm shelf water to the glacier terminus enabled increased submarine melt and subsequent glacier acceleration (e.g., Beaird et al., 2017; Motyka et al., 2003; Straneo et al., 2010; Sutherland & Straneo, 2012). Both the speed of circulation and temperature of ocean water in contact with the glacier terminus are major contributors to enhanced subma-

rine melting and subsequent calving of the glacier terminus (O'Leary & Christoffersen, 2013; Schild et al., 2018; Slater et al., 2018); therefore, quantifying fjord circulation is a critical component in assessing the impact of ocean water on tidewater glacier retreat.

Fjords serve as the primary pathway between tidewater glaciers and the ocean, where mixing between glacier discharge (icebergs, meltwater) and ocean water occurs. Fjord circulation is often modeled as two-layer estuarine flow (Farmer & Freeland, 1983; Stigebrandt, 2012), with the surface layer transporting glacially modified freshwater to the shelf and the bottom layer transporting warm saline ocean water to the glacier terminus (e.g., Cowton et al., 2015; Davison et al., 2020; Sutherland, Straneo, & Pickart, 2014). Numerical models have successfully modeled overall fjord circulation (Carroll et al., 2015; Cowton et al., 2015; Klinck et al., 1981; Salcedo-Castro et al., 2011), the impact of glacier meltwater runoff on fjord circulation and freshening (e.g., Cowton et al., 2015; Davison et al., 2020; Slater et al., 2018; Sutherland & Straneo, 2012), quantified heat transport (e.g., Sutherland & Straneo, 2012), and fjord circulation strength (Slater & Straneo, 2022; Slater et al., 2018; Xu et al., 2013). However, models are limited by the spatial resolution of model inputs (i.e., bathymetry data) as well as the resolution of the model itself (Zhao et al., 2021) making smaller features of fjord geometry difficult to include. Tributary fjords are often narrower and shallower than the main fjord, creating gaps in the availability of high resolution bathymetry products (i.e., BedMachine v3, 150 m, Morlighem et al., 2017) as well as discontinuities in horizontal and vertical fjord resolution within the model; therefore, tributary fjords are challenging to incorporate, and fjord systems are often simplified to a 2D centerline approach (Straneo et al., 2011; Sutherland, Straneo, & Pickart, 2014). However, recent non-glaciated estuary studies have found that tributary inflow exerts a strong influence on circulation, speed, and stratification within the main estuary trunk (e.g., Garcia et al., 2021; Gong et al., 2020), and therefore tributaries are a necessary component when considering overall fjord circulation.

In this study we use icebergs as natural drifters to measure upper-layer (<250 m) fjord circulation (Schild et al., 2018; Sutherland, Roth, et al., 2014) in regions of the fjord containing freely floating icebergs (i.e., outside the mélange region). We deploy GPS trackers on 13 icebergs in Ilulissat Icefjord (Figure 1) in the summers of 2014 and 2019, capturing hourly variations in iceberg speed and trajectory. To isolate motion due solely to fjord circulation, we account for additional influences on iceberg movement including strong winds, surrounding ice, and glacier behavior (Sutherland, Roth, et al., 2014; Wagner et al., 2017), as well as test the applicability of other influence (e.g., Coriolis, standing eddies; Zhao et al., 2023) on iceberg trajectory. In using a combination of remote sensing, reanalysis output, and in situ measurements, we isolate the fjord circulation response to tributary fjord runoff.

2. Study Area

This study focuses on the upper-layer (0–250 m) circulation in Ilulissat Icefjord, west Greenland. Ilulissat Icefjord borders the terminus of Sermeq Kujalleq (catchment basin: 101,187 km^2), the fastest glacier and most prolific producer of icebergs in Greenland (Joughin et al., 2008). Ilulissat Icefjord is ∼58 km long, ranges between 5 and 13 km wide, and reaches a depth of ∼800 m between the shallow sill (∼245 m deep) and glacier terminus (Figure 1; Gladish et al., 2015; Morlighem et al., 2017). In a simplified two-dimensional scenario, dense ocean water enters Ilulissat Icefjord by spilling over the shallow sill at the fjord mouth (Figure 1b), entraining basin waters and mixing as it descends. This mixed ocean water then continues flowing toward the glacier terminus at the depth where it reaches neutral buoyancy, where depth is dependent upon the densities of the various water masses (e.g., Cenedese & Adduce, 2010). At the glacier terminus, the mixed ocean water is entrained in subglacial freshwater discharging at depth and buoyantly rises toward the fjord surface. As this freshwater plume rises, the entrained warm ocean water is brought directly in contact with the glacier terminus, contributing to additional terminus melt (convective and ambient melt; Cenedese & Gatto, 2016; Slater et al., 2018). The plume continues to buoyantly rise until reaching equilibrium (e.g., Jenkins, 2011), and then flows down-fjord (influenced by bathymetry, wind, iceberg presence, and shelf flow; Davison et al., 2020; Hager et al., 2022; Kajanto et al., 2022; Zhao et al., 2022) until entering the ocean (Figure 1b). While the majority of freshwater in Ilulissat Icefjord originates as subglacial discharge, meltwater also results from the abundance of icebergs in the fjord, and to a much lesser degree, the convective and ambient melting of the terminus.

The bathymetry and geometry of Ilulissat Icefjord play a dominant role in its unique fjord hydrography. The shallow sill constrains fjord-shelf water exchange above the sill (Gladish et al., 2015; Sutherland, Straneo, & Pickart, 2014), trapping water on the leeward side (Beaird et al., 2017; Stigebrandt, 2012), which in turn obstructs

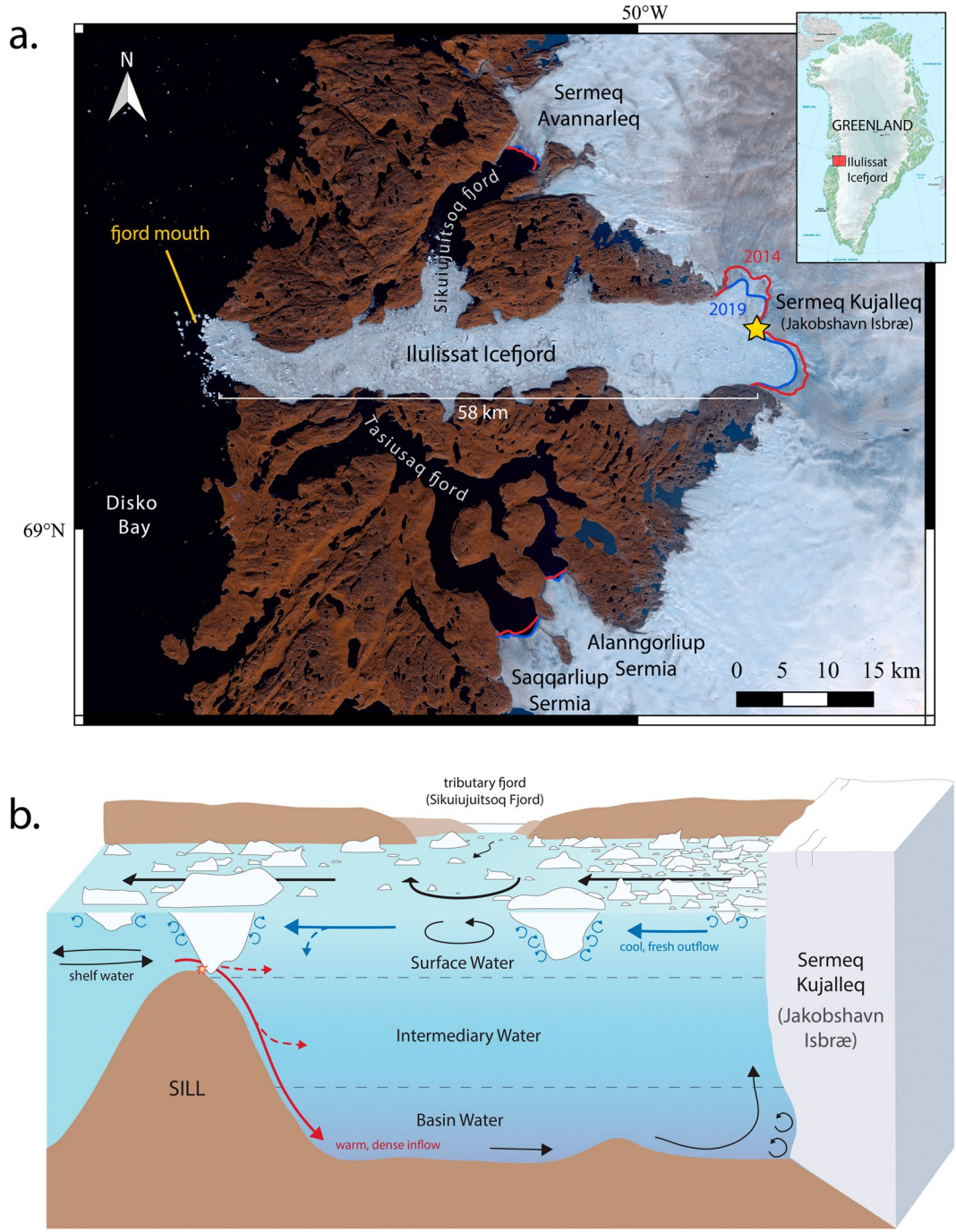

Figure 1. Ilulissat Icefjord, west Greenland with tributary fjords and glaciers labeled in map view (a) and water layers shown in the schematic transect view (b). Terminus positions for 2014 (red) and 2019 (blue) are delineated in the map view, with the yellow star representing the location of Sermeq Kujalleq terminus position for measurements in this study. Schematic of Ilulissat Icefjord depicts the inflow of warm, dense ocean water (red arrow), mixing of water at the glacier terminus (black arrows), and outflow of cool, fresh, glacially modified water (blue arrows). The confluence location of the northern tributary fjord (Sikuiujuitsoq Fjord) is noted, as well as the three primary water masses (named) and circulation patterns (thick black arrows). Background image (a) from Landsat 8, collected 25 August 2019.

density-driven circulation and strongly influences the flow of water (e.g., Beaird et al., 2017; Davison et al., 2020; Hager et al., 2022; Kajanto et al., 2022). The shallow sill also acts as a physical barrier to deep-keeled icebergs, forcing them to break apart at the fjord mouth (Beaird et al., 2017) prior to entering Disko Bay and the open

ocean. Further, the presence of tributary fjords act as additional freshwater injection locations, with the timing, magnitude, and velocity of meltwater delivery dependent upon the resident tidewater glacier at the head of each fjord. These tributary tidewater glaciers include Sermeq Avannarleq (catchment basin: ~423 km^2; via Sikuiujuitsoq Fjord), Saqqarliup Sermia, and Alanngorliup Sermia (catchment basins: ~199, ~3,544 km^2; via Tasiusaq Fjord; Figure 1a).

3. Methods

3.1. Iceberg Movement

To quantify iceberg speed and trajectory, we deployed expendable GPS units by helicopter on 13 large (>250 m surface length) icebergs; eight icebergs in 2014 (Globalstar Axonn AXTracker, lat-lon ±20 m; Sutherland, Roth, et al., 2014) and five icebergs in 2019 (Globalstar SmartOne C, lat-lon ±10 m; Schild et al., 2021). The expendable GPS units relayed hourly iceberg position (*lat-lon*) to an offline server from mid-August (15 August 2014, 12 August 2019) through iceberg capsize and/or loss of signal (+8–127 d). To transform iceberg position into measurements of depth-averaged currents, we used simple forward differencing of the hourly positions. To estimate iceberg volume and keel depth, we used a combination of three-dimensional sail geometries and established empirical relationships between surface and subsurface features (Schild et al., 2021). Three-dimensional sail geometries were constructed by applying structure from motion (SfM) processing on multiple camera images collected during GPS helicopter deployment (five icebergs, 2019). Imagery was collected in a single pass circling the iceberg from above (using a DSLR Pentax K100D Super camera), and georeferenced using a handheld GPS (Garmin GPSMAP 62s). In instances without adequate or sufficient camera imagery to apply SfM processing (eight icebergs, 2014), a combination of WorldView-derived DEMs (3D) and high-spatial resolution satellite imagery (2D; Worldview-3 and Landsat 8) was used. This combined approach generated sail geometry for all but one iceberg (IF0614, 2014), due to a lack of imagery during the short iceberg survival period (8 days). Keel depths were estimated using a derived ~2:1 ratio of surface length to keel depth, based on the maximum surface length of each iceberg (Schild et al., 2021). Projected total volume was calculated from the 2014 DEMs and 2019 DSMs using atmospheric pressure (DMI AWS #4221; Cappelen, 2021), average fjord hydrography measurements (Beaird et al., 2017), and an ice density of 917 kg m^{-3} (Table S1 in Supporting Information S1).

3.2. Fjord Hydrography

Fjord hydrographic conditions were calculated using conductivity, temperature, and depth (CTD) measurements, bin-averaged in 1-m intervals from the surface to ~800 m depth. Profiles were collected by helicopter within the fjord (eight X-CTD profiles in 2014; seven X-CTD profiles in 2019) or by ship just outside Ilulissat Icefjord in Disko Bay (five CTD profiles in 2014: RBR XR-620; seven profiles in 2019: RBRconcerto). Profiles were collected during on-iceberg GPS deployment campaigns (15 August 2014, 12 and 13 August 2019). These data were used to characterize fjord water masses through temperature and salinity measurements, and calculate average water density with depth to enable projected iceberg volume calculations.

3.3. Meltwater Input

To constrain the influence of glacier meltwater runoff on surface circulation in Ilulissat Icefjord, we calculated the volume, location, and subglacial transit time of meltwater runoff from all tidewater glaciers draining into Ilulissat Icefjord (e.g., Rennermalm et al., 2013). As direct measurements of tidewater glacier meltwater runoff are not currently feasible due to multiple discharge locations at depth and immediate dispersion of runoff within the water column (Cenedese & Gatto, 2016; Felikson et al., 2017; Lindbäck et al., 2018), we derived glacier runoff using the RACMO 2.3p2 runoff product (Noël et al., 2016). We first established hydrologic catchment basins for each of the four tidewater glaciers (Sermeq Kujalleq, Sermeq Avannarleq, Saqqarliup Sermia, and Alanngorliup Sermia) draining into Ilulissat Icefjord using the 90 m Greenland Ice Sheet Mapping Project (GIMP) DEM (Howat et al., 2015). We then isolated daily runoff in RACMO 2.3p2 for each catchment basin and applied a time delay to account for the transit time from the meltwater genesis location to the glacier terminus (1.0 m s^{-1} subglacial flow velocity; Cowton et al., 2013). To account for the transit time of meltwater originating from glaciers in tributary fjords to Ilulissat Icefjord, we applied a time delay based upon the arrival of the runoff-induced velocity pulse (1.1 m s^{-1} surface velocity of subglacial discharge plume; Slater et al., 2018).

Recent modeling work has shown that the subglacial discharge water mass itself may have a longer residence time, upwards of a month, in the near-terminus environment (Sanchez et al., 2023); however, in this study, we focus on surface velocities resulting from meltwater runoff (water displacement) not the water mass itself, and therefore apply a more representative transit time to calculate runoff-induced pulse arrival in Ilulissat Icefjord. A sensitivity analysis using a range of previously measured transit times in similar environments (subglacial: 0.5–1.2 m s^{-1}, Cowton et al., 2013; down fjord: 0.2–2.0 m s^{-1}, Slater et al., 2018), showed variability in arrival time to be within the temporal resolution of the overall study (1 d), supporting the use of singular average values for subglacial and down-fjord transit times. To establish a time series of increased periods of meltwater flux (meltwater runoff pulses), we calculated meltwater runoff anomalies, using the average runoff volume during the summer melt season (July–mid October) as the baseline.

3.4. Additional Contributing Variables

In addition to fjord circulation, iceberg speed and trajectory can also be influenced by calving events, glacier movement, and wind (Amundson et al., 2010; Cassotto et al., 2015, 2021; Sutherland, Roth, et al., 2014; Wagner et al., 2017). To examine the impact of these confounding variables on iceberg movement, we quantified the contribution of each variable by constructing time series of calving events, glacier velocity, and wind speed and direction. To construct a calving time series, we focused solely on glacial calving into Ilulissat Icefjord and not the tributary fjords. Following the methods of prior studies, we used a combination of satellite imagery (Landsat 8, MODIS, and Sentinel-1), maximizing spatial and temporal resolution, and manually digitized the glacier terminus position within a standardized box (Moon & Joughin, 2008). We then divided the area by the box width to achieve a width-normalized terminus position (Schild & Hamilton, 2013). To construct a glacier velocity time series, we used the Sermeq Kujalleq mean monthly MEaSUREs Greenland ice velocity data set between August and October for 2014 and 2019 (Howat, 2020), and created two subsets of velocity results for each year, to better account for the impact of glacier movement. In the first subset, we collected a centerline transect focused on the velocity transition from ~19.5 km up-glacier, through the terminus, into the mélange. In the second subset, we focused on overall glacier terminus velocity, by extracting average velocities in a 7 km^2 region, just up-glacier (~0.4–1 km) from the terminus. Lastly, to construct the wind speed and direction time series, we used the automated weather station (AWS) at Ilulissat Airport, ~5 km from Ilulissat Icefjord (DMI AWS #04221; Cappelen, 2021), where wind speed and direction (±0.01 m s^{-1}) were collected hourly and averaged to construct a daily time series.

4. Results

4.1. Iceberg Trajectories

During the 2014 and 2019 field campaigns, a total of 13 on-iceberg GPS units were deployed, remaining active 8–127 days (2014 average: 44, range ±36 d; 2019 average: 100, range ±27 d; Table 1), and transiting 4–150 km away from the terminus (2014 average: 82.1 ± 60.0 km; 2019 average: 51.3 ± 49.4 km; Table S1 in Supporting Information S1) before loss of signal. Of the 13 instrumented icebergs, eight icebergs maintained communication throughout Ilulissat Icefjord and moved into Disko Bay (Figures 2a and 2b) while five lost communication within Ilulissat Icefjord (Table S2 in Supporting Information S1). Across the entire fjord, the 2014 iceberg trajectories record average down-fjord velocities three times greater in 2014 than those in 2019, and average residence times a quarter of those in 2019 (Table 1, Figure 3), however there is significant variability in iceberg movement and behavior within the fjord. During the instrumental period, iceberg movement fell into one of three categories, which subsequently defined distinct, but spatially variable, regions in Ilulissat Icefjord. We identify these fjord regions as (a) mélange (terminus to 25 ± 7 km down-fjord), (b) mid-fjord (end of mélange to 44 ± 1 km down-fjord), and (c) fjord mouth (end of mid-fjord to the fjord mouth, at 58 km down-fjord; Figures 2e and 2f).

The mélange region is characterized by a tightly packed configuration of icebergs and sea ice, where iceberg movement is directly down-fjord and synchronous across-fjord. During calving events (width-normalized terminus retreat of 0.05–0.2 km; Figures 2c and 2d), instrumented icebergs in the mélange region all recorded large synchronous advances in position (~0.6–4 km) and short duration (~1–3 hr) spikes in speed (<1–80 m d^{-1}). In 2014, the mélange region was about half as long in overall length (18 km) than in 2019 (32 km), with the 2014 icebergs moving nearly four times as quickly ($1.98 \pm 0.45 \times 10^3$ m d^{-1} vs. $0.48 \pm 0.15 \times 10^3$ m d^{-1}; Table 1) and

Journal of Geophysical Research: Oceans
10.1029/2023JC020117

Table 1
Iceberg Geometry and Behavior During the 2014 and 2019 Campaigns

Iceberg		Surface length (m)	Est. keel depth (m)	Volume ($\times 10^5$ m^3)		Residence time (days)				GPS transit time (d)	Avg. Velocity ($\times 10^3$ m d^{-1})		
				Surface	Projected total	Mélange	Mid-fjord	Fjord mouth	Ilulissat Icefjord		Mélange	Mid-fjord	Fjord mouth
IF0114		380	190	–	–	–	13	4	17	44	–	4.94	3.20
IF0214		366	183	–	–	–	6	8	14	71	–	6.56	2.19
IF0314		628	314	–	–	–	10	11	21	37	–	4.28	1.47
IF0414		480	240	21.9	203.0	5	11	27	43	43	2.74	3.00	1.67
IF0514		1,000	500	–	–	10	1	–	11	11	1.65	1.02	–
IF0614	–	–	–	–	–	8	–	–	8	8	2.01	–	–
IF0714		377	188	8.5	79.0	14	13	2	29	71	1.77	3.09	3.93
IF0814		283	141	–	–	10	9	5	24	71	1.73	3.26	1.77
2014 Average:		**502**	**251**	**15.2**	**141.0**	**9.4 ± 3.2**	**9.0 ± 4.3**	**9.5 ± 9.1**	**20.9 ± 11.2**	**44.5 ± 25.7**	**1.98 ± 0.45**	**3.74 ± 1.75**	**2.37 ± 0.98**
IF0719		399	199	4.5	41.9	106	–	–	106	106	0.25	–	–
IF0819		972	486	123.0	1,150.0	93	–	–	93	93	0.42	–	–
IF0919		759	379	125.0	1,170.0	42	40	–	82	82	0.63	0.68	–
IF1019		381	190	4.8	45.6	18	26	30	74	93	0.59	0.88	0.97

Table 1
Continued

Iceberg		Surface length (m)	Est. keel depth (m)	Volume ($\times 10^5$ m^3)		Residence time (days)				GPS transit time (d)	Avg. Velocity ($\times 10^3$ m d^{-1})		
				Surface	Projected total	Mélange	Mid-fjord	Fjord mouth	Ilulissat Icefjord		Mélange	Mid-fjord	Fjord mouth
IF1119		447	223	14.8	139.0	42	10	62	114	127	0.51	2.70	0.78
2019 Average:		**592**	**296**	**54.3**	**509.0**	**60.2 ± 37.5**	**25.3 ± 15.0**	**46.0 ± 22.6**	**87.2 ± 16.5**	**100.2 ± 17.2**	**0.48 ± 0.15**	**1.42 ± 1.11**	**0.88 ± 0.13**

Note. Iceberg surface length was measured from Worldview-3 and Landsat 8 (only IF0214) imagery in 2014, and SfM-derived point clouds (DSMs) in 2019, aside from IF0614 where there is no available imagery. Estimated keel depth is based on the empirical surface length:keel depth relationship (~2:1; Schild et al., 2021). Iceberg surface volume was measured using DEMs (2014) and DSMs (2019), and projected total volume was calculated using surface volume measurements and accounting for air pressure (DMI AWS) and ocean water density (CTD and X-CTD casts; Table S1 in Supporting Information S1). Average velocity by fjord section was calculated using on-iceberg GPS positions, with standard deviations noted for residence time, transit time, and average velocities. Bold values represent column averages for 2014 and 2019.

advancing farther during calving events (up to 4 km vs. up to 2 km) than those in 2019. This resulted in a shorter residence time in 2014 (9.4 ± 3.2 d; normalized by region length: 1.0 ± 0.6 d km^{-1}) than in 2019 (60.2 ± 37.5 d; normalized by region length: 4.1 ± 2.6 d km^{-1}; Table 1; Table S2 in Supporting Information S1).

The mid-fjord region is characterized by freely floating icebergs, with changes in velocity independent of glacier speed and timing of calving events. Opposite of the mélange region extent, the mid-fjord region extended farther in 2014 (27 km) than in 2019 (11 km), with icebergs again moving more quickly (3.74 ± 1.71 × 10^3 m d^{-1} vs. 1.42 ± 1.11 × 10^3 m d^{-1} in 2019). This increased 2014 velocity in comparison to 2019 also resulted in a shorter residence time in 2014 (9.0 ± 4.3 d; normalized by region length: 0.6 ± 0.3 d km^{-1}) than in 2019 (25.3 ± 15.0 d; normalized by region length: 1.3 ± 1.0 d km^{-1}; Table 1; Table S2 in Supporting Information S1). Iceberg movement through areas abutting the confluence of tributary fjords (Sikuiujuitsoq Fjord from the north, Tasiusaq Fjord from the south), fell into one of two subcategories: icebergs either continued straight down-fjord (four icebergs) or deviated from the down-fjord trajectory (five icebergs), pushing south (2019, two icebergs) or reversing direction and moving up-fjord (2014, three icebergs) before regaining the original down-fjord trajectory. In 2019, instrumented icebergs that did deviate at the confluence, first deflected south at the Sikuiujuitsoq Fjord tributary outflow and then north at the Tasiusaq tributary outflow. Once past these confluences, and in the fjord mouth region, the icebergs return to the northern boundary outflow (Figures 2e and 2f). The occurrence of a deviation was independent of iceberg size (Table 1), however the timing and location of deviation coincided with the timing of increased runoff from respective tributary fjords (Section 4.3).

The fjord mouth region extended 13 (2014)–15 (2019) km, from the mid-fjord region to the mouth of Ilulissat Icefjord (58 km from terminus), and is again characterized by freely floating icebergs, where changes in iceberg velocity are independent of glacier speed and the timing of calving events. Contrasting the mid-fjord region however, iceberg trajectory in the fjord mouth region was solely down-fjord without deviation. Icebergs in this region again transited more quickly in 2014 (2.37 ± 0.98 × 10^3 m d^{-1}) than in 2019 (0.88 ± 0.13 × 10^3 m d^{-1}), and subsequently also remained in the fjord mouth region for less time (9.5 ± 9.1 d vs. 46.0 ± 22.6 d in 2019; normalized by region length: 0.7 ± 0.7 d km^{-1} vs. 2.3 ± 1.5 d km^{-1} in 2019; Table 1; Table S2 in Supporting Information S1).

4.2. Glacier Velocity

Overall, Sermeq Kujalleq near-terminus velocities were faster in 2014 by 6 m d^{-1} (25 m d^{-1}) than in 2019 (19 m d^{-1}; Figure 4), however, differences were not spatially uniform. The centerline transect spans the glacier-mélange transition, which is generally the fastest region of a tidewater glacier, and the slowest region of the mélange (most tightly packed). At this transition, there is an increase in speed by 38% (2019)–51% (2014) when transitioning from the mélange to the glacier. Moving away from this transition, the glacier decreases speed 1.3 (2019)–1.8 (2014) m d^{-1} with each kilometer up glacier from the terminus, while the mélange increases speed one (2019) to two (2014) orders of magnitude as it moves toward the mid-fjord region. The 2014 centerline transect values from August to October are ~30% faster than in 2019, which coincides with faster ice velocities near the calving front and a faster mélange region (1.98 × 10^3 m d^{-1} vs. 0.48 × 10^3 m d^{-1} in 2019; Table 1). While the average near-terminus velocity of Sermeq Kujalleq varied between years, the trend in velocity change across the mélange-glacier transition remained consistent (Figure 4).

4.3. Meltwater Runoff

The magnitude and timing of meltwater runoff delivery to Ilulissat Icefjord (via water displacement) varies both within and between the 2014 and 2019 summer–winter seasons (July–December). During the meltwater runoff observational period (July–December), meltwater delivery peaked in late July (57.5 × 10^7 m^3 d^{-1} on 31 July 2019) and mid-August (46.2 × 10^7 m^3 d^{-1} on 17 August 2014), declining through September, with low delivery from October to December (<0.2 × 10^7 m^3 d^{-1}; Figure 5).

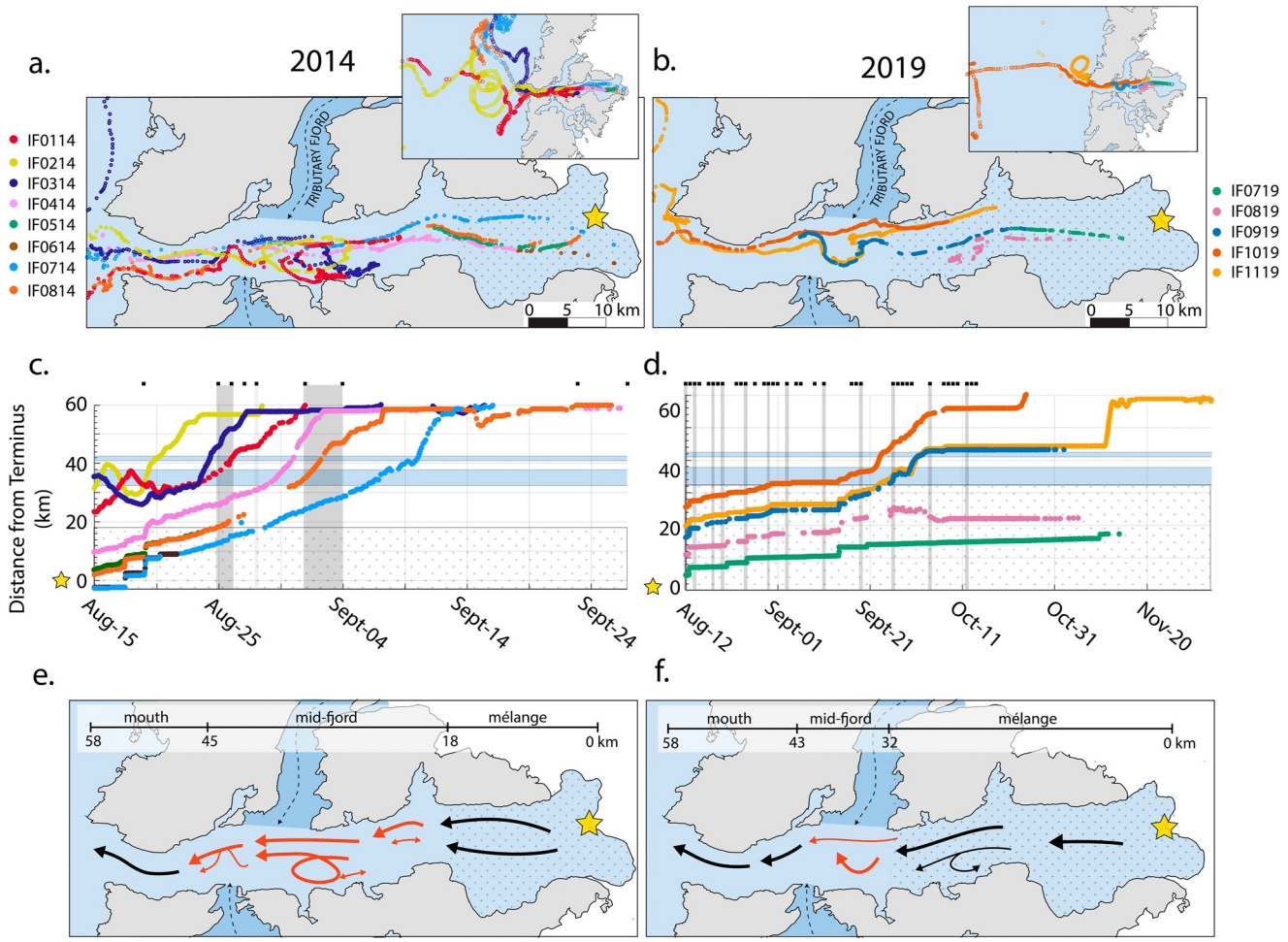

Figure 2. Iceberg position and movement in Ilulissat Icefjord for 2014 (left column) and 2019 (right column). The top panels (a, b) show individual iceberg paths in Ilulissat Icefjord. The middle panels (c, d) show time series of iceberg distance from the terminus (yellow star), with colored bands representing the confluence location of tributary fjords (dark blue), the mélange region (dotted pattern), and instances of large calving events (gray; available terminus position data noted as black circles). The bottom panels (e, f) show schematics of general iceberg trajectory (black arrows) with the mid-fjord region trajectory highlighted by orange arrows. Arrow thickness represents the relative popularity of each trajectory, and deashed arrows represent likely tributary outflow direction.

During the 2014 and 2019 instrumental period, meltwater runoff delivery spanned 0–57.5 × 10^7 m^3 d^{-1}, with the meltwater runoff peak in 2014 overlapping with iceberg deployment. Meltwater runoff delivery was variable, with episodic periods of increased meltwater runoff delivery (355%–1,059% above background volumes) lasting 1–5 days (hereafter referred to as runoff pulses). These runoff pulses were an order of magnitude greater in 2014 (reaching 10.0 × 10^7 m^3 d^{-1}) than in 2019 (reaching 0.8 × 10^7 m^3 d^{-1}), which also coincides with faster Sermeq Kujalleq velocities and shorter iceberg residence times.

4.4. Fjord Temperature and Salinity

Fjord hydrography measurements from CTD and X-CTD casts (via two similar but not identical fjord transects; Figures 6a and 6b) show three distinct water masses in Ilulissat Icefjord; we identify these as surface water (upper 50 m), intermediary water (~50–500 m), and basin water (>400 m; Figure 6). The surface water is cool and fresh (<0.7°C; <32 PSU), and is situated above the intermediate water, which is warmer and more saline (~2.0–2.5°C; 32–34 PSU). Basin water, situated below the intermediate water, becomes increasingly warmer and more saline with depth (>3.0°C; >34 PSU), and is most consistent with Atlantic Water (Figure 6; Everett et al., 2018; Straneo et al., 2011; Sutherland, Straneo, & Pickart, 2014). Within the surface water mass, salinity and temperature vary with distance from the terminus; closest to the terminus, the coolest and freshest water is found, with both temperature and salinity increasing with distance down-fjord. While the intermediary layer is relatively consistent

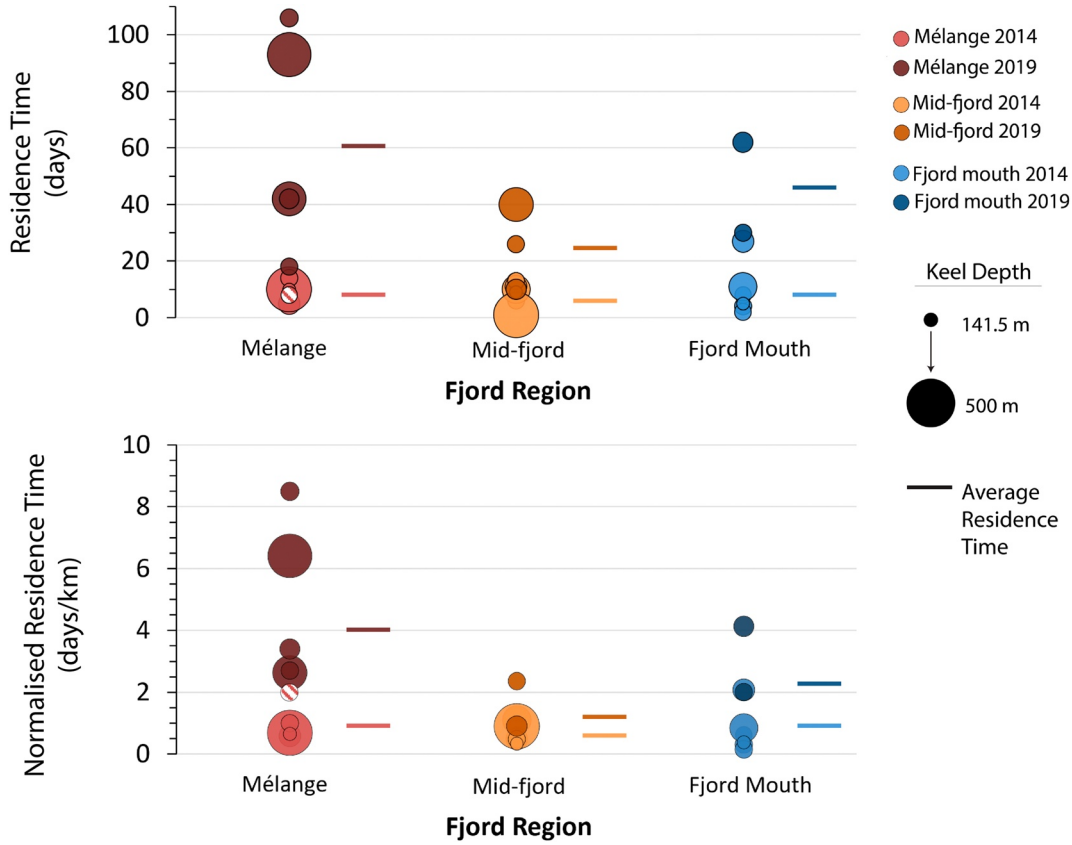

Figure 3. Iceberg residence time (a) and residence time normalized by horizontal distance traveled in that region (b) for each instrumented iceberg in the three defined fjord regions for 2014 (lighter colors) and 2019 (darker colors). Each circle diameter is scaled to iceberg keel depth, with the striped circle representing iceberg IF0614 (unknown keel depth). Horizontal bars to the right of circles represent the average iceberg residence time for each fjord region.

in temperature and salinity throughout the fjord, the basin layer again varies with distance from the terminus, with warmer and more saline waters located down-fjord (i.e., near the sill). Interannually, there is variability in the salinity, temperature, and extent of the individual water masses. In 2014, Ilulissat Icefjord waters were warmer and more saline, with average temperatures ∼0.5°C warmer and average temperatures more saline in the surface (0.2 PSU) and intermediary (0.6 PSU) water masses, and ∼1.5°C warmer and 0.1 PSU more saline in the basin water mass. The coolest water within the surface water mass remained closer to the glacier terminus (within the mélange to mid-fjord region vs. extending the full length of the fjord in 2019; Figures 6c–6f), and the warmer and more saline basin water mass was ∼100 m thicker with an intermediary water-basin water transition at about 400 m depth (vs. 500 m depth in 2019). While the interannual differences in temperature, salinity, and stratification are sizable, these results are consistent with previous work focused on the impact of mélange on fjord hydrography as iceberg presence is shown to alter upper layer hydrography toward cooler and fresher conditions (Davison et al., 2020; Hager et al., 2022; Kajanto et al., 2022).

4.5. Wind Events

The instrumented icebergs in this study fall into the size classification of "small" (<1.5 km in length, Wagner et al., 2017), making them susceptible to transport by strong winds (>>2.17–7.69 m s^{-1}; using Wagner et al., 2017, Equation 13) in the along-fjord direction. In both 2014 and 2019, wind speeds below 9 m s^{-1} were multidirectional, however a majority (62%) of the strongest winds (9–14.6 m s^{-1}) originated from the east (Figure S1 in Supporting Information S1) and, if influential, would move icebergs in the along-fjord direction. To evaluate the influence of wind events on the trajectory of freely floating icebergs (i.e., icebergs in the mid-fjord and fjord mouth regions) during the survey period, we compared the iceberg speed during identified wind events

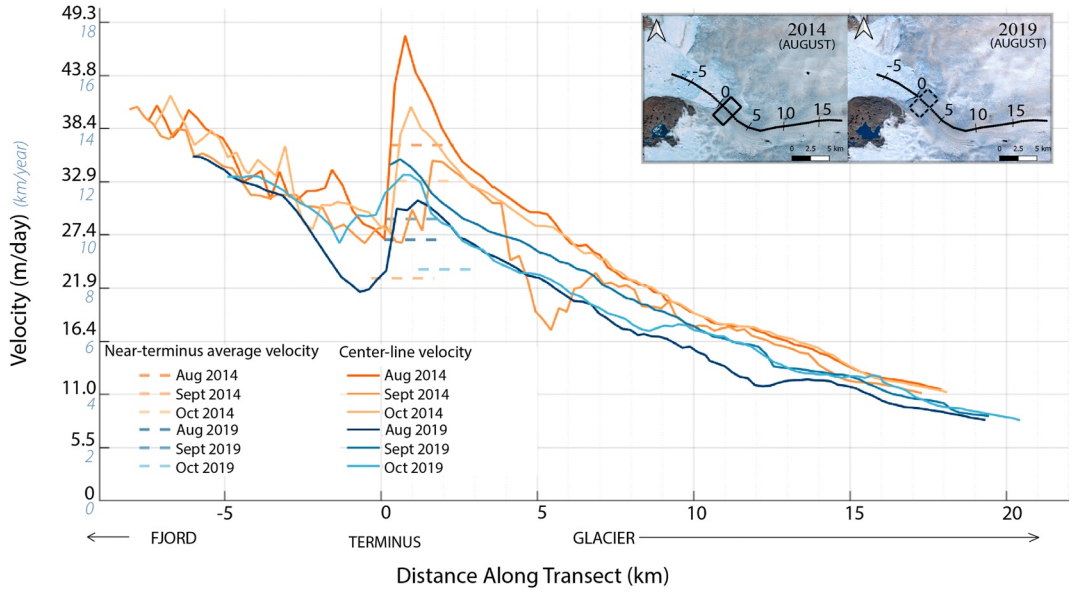

Figure 4. Monthly fall (A, S, O) glacier and mélange velocities for Sermeq Kujalleq in 2014 (oranges) and 2019 (blues) using the MEaSUREs Greenland Ice Velocity data set (Howat, 2020). Centerline transect velocities (solid lines) span the mélange region of the fjord to ~17–19 km up glacier, and average near-terminus velocities (dashed lines) cover a 2 by 3.5 km region up-glacier (inset, box).

(defined as >9 m s^{-1}) to the background iceberg speed (average of ±2 hr surrounding the wind event), and also compared the occurrence of iceberg speed anomalies (calculated by region) to the time series of wind events. During the 39 identified wind events (Figure S2 in Supporting Information S1), iceberg speeds changed between −0.12 and 0.25 m s^{-1} (−120%–9,700%; Figure 7) irrespective of iceberg size (Figures S3 and S4 in Supporting Information S1). Of these speed changes, only 37% equated to >2% wind speed (22% mid-fjord and 33% in

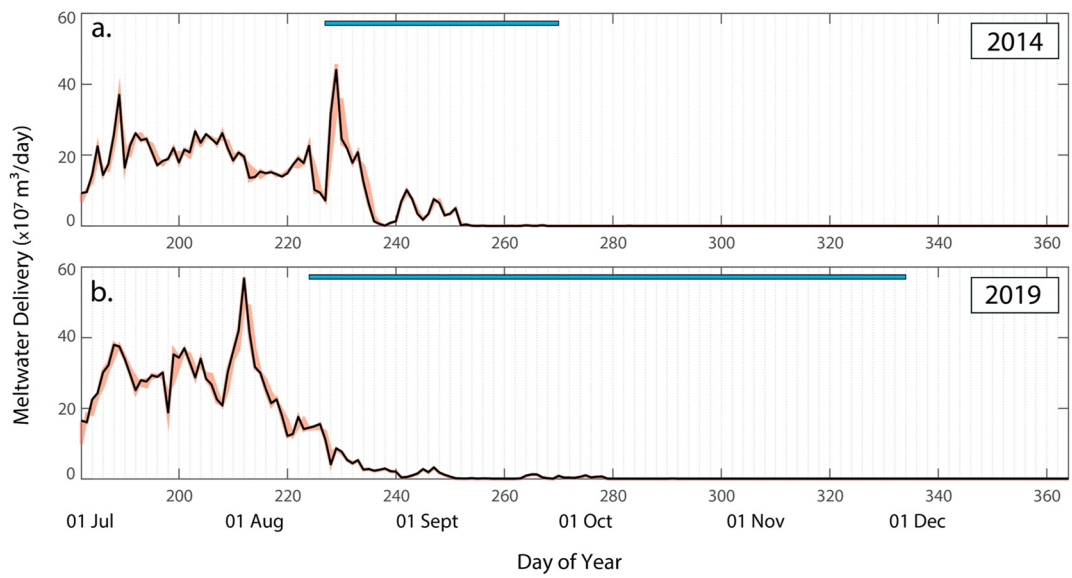

Figure 5. Hydrograph of meltwater runoff delivery (via water displacement) from tidewater glaciers to Ilulissat Icefjord between 01 July and 31 December 2014 (a) and 2019 (b). Meltwater runoff delivery was calculated by applying subglacial (1.0 m s^{-1}) and down-fjord (1.1 m s^{-1}) transit delays to daily glacier meltwater runoff volumes. The potential variability in delivery time is noted by orange shading (subglacial: 0.5–1.2 m s^{-1}; Cowton et al., 2013, down-fjord: 0.2–2.0 m s^{-1}; Slater et al., 2018). The horizontal blue bars represent the period of time the instrumented icebergs were transiting in Ilulissat Icefjord.

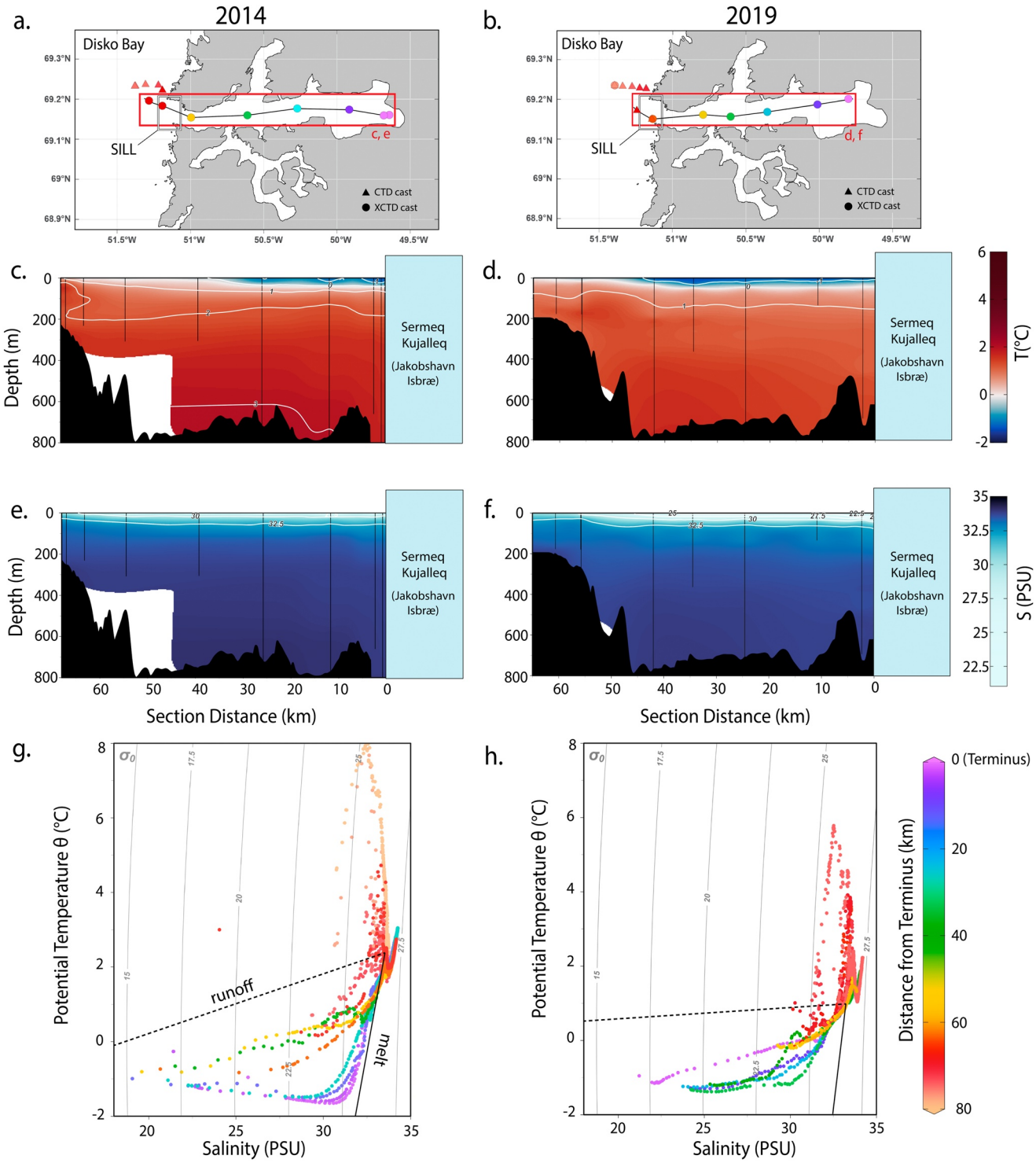

Figure 6. Location of CTD (triangles) and X-CTD (circles) casts in Ilulissat Icefjord for 2014 (a) and 2019 (b), colored by distance from terminus, with temperature (c, d) and salinity (e, f) results shown. Black vertical lines (c–f) represent the location and depth of each cast, white areas are locations with no data, and black areas show the bathymetry along each transect (GEBCO, 2020). Due to iceberg abundance, exact resampling was not possible and therefore the transect line varies slightly between years. Temperature and salinity are shown in temperature-salinity (T-S) space for 2014 (g) and 2019 (h), with color designating distance from terminus, and isopycnals (light gray solid line), submarine melt (black solid line), and subglacial runoff (black dashed line) noted.

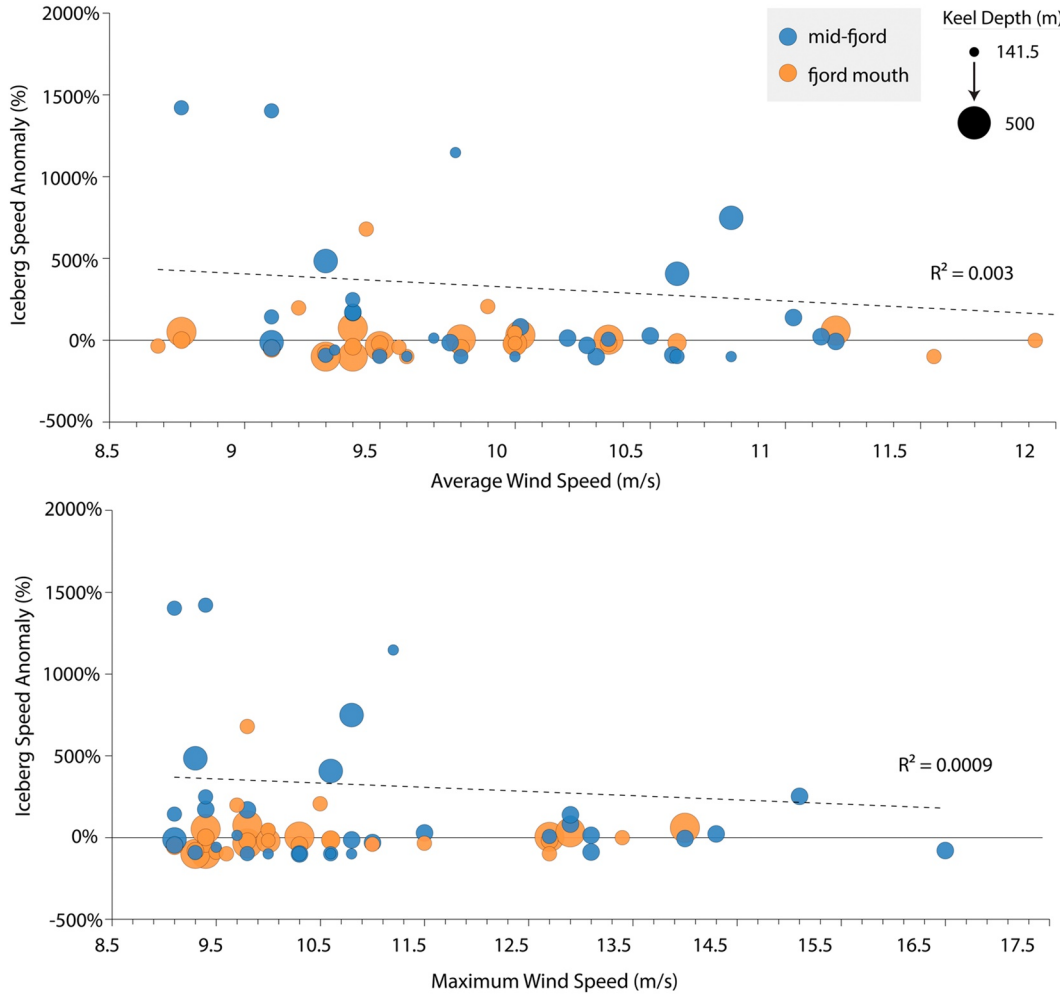

Figure 7. Iceberg speed anomaly during wind events (>9 m s^{-1}) as a function of average (top) and maximum (bottom) wind speed during the 2014 and 2019 campaigns. Circle diameter is scaled to iceberg keel depth, with colors representing fjord region at time of associated wind event. For ease of visibility, two outlier data points are not included in the above plots but are included in calculations and in Figure S6 of the Supporting Information S1.

fjord mouth regions). Of the 23 identified iceberg speed anomalies, only 8 coincided with wind events (Figure 7; Figure S5 in Supporting Information S1). While these results do not dismiss the influence of wind, they do point toward additional variables with greater influence on iceberg speed in this environment.

5. Discussion

In this study we identify three distinct fjord regions based upon different iceberg behavior, and propose two primary drivers of upper-layer circulation in Ilulissat Icefjord: (a) glacier behavior (calving and glacier speed) in the mélange region, and (b) meltwater runoff delivery (via water displacement) in the mid-fjord and fjord mouth regions. Iceberg movement in the mélange region is characterized by slow persistent down-fjord movement interrupted by large, fjord-wide, synchronous, and immediate advances in iceberg position down-fjord. The slow persistent movement scales with glacier velocity (one to two orders of magnitude larger than glacier velocity in 2019 and 2014, respectively), while the rapid advances coincide with large calving events (identified during periods of image availability; Figure 2). However, while both katabatic winds and meltwater runoff from Sermeq Kujalleq would accelerate icebergs in the down-fjord direction, we did not observe any discernible change in position coinciding with the timing of these wind events (Figure S2 in Supporting Information S1) or peaks in Sermeq Kujalleq meltwater runoff (Figure S7 in Supporting Information S1), suggesting that these are not dominant controls in the mélange region. These results are consistent with prior studies at Sermeq Kujalleq, which

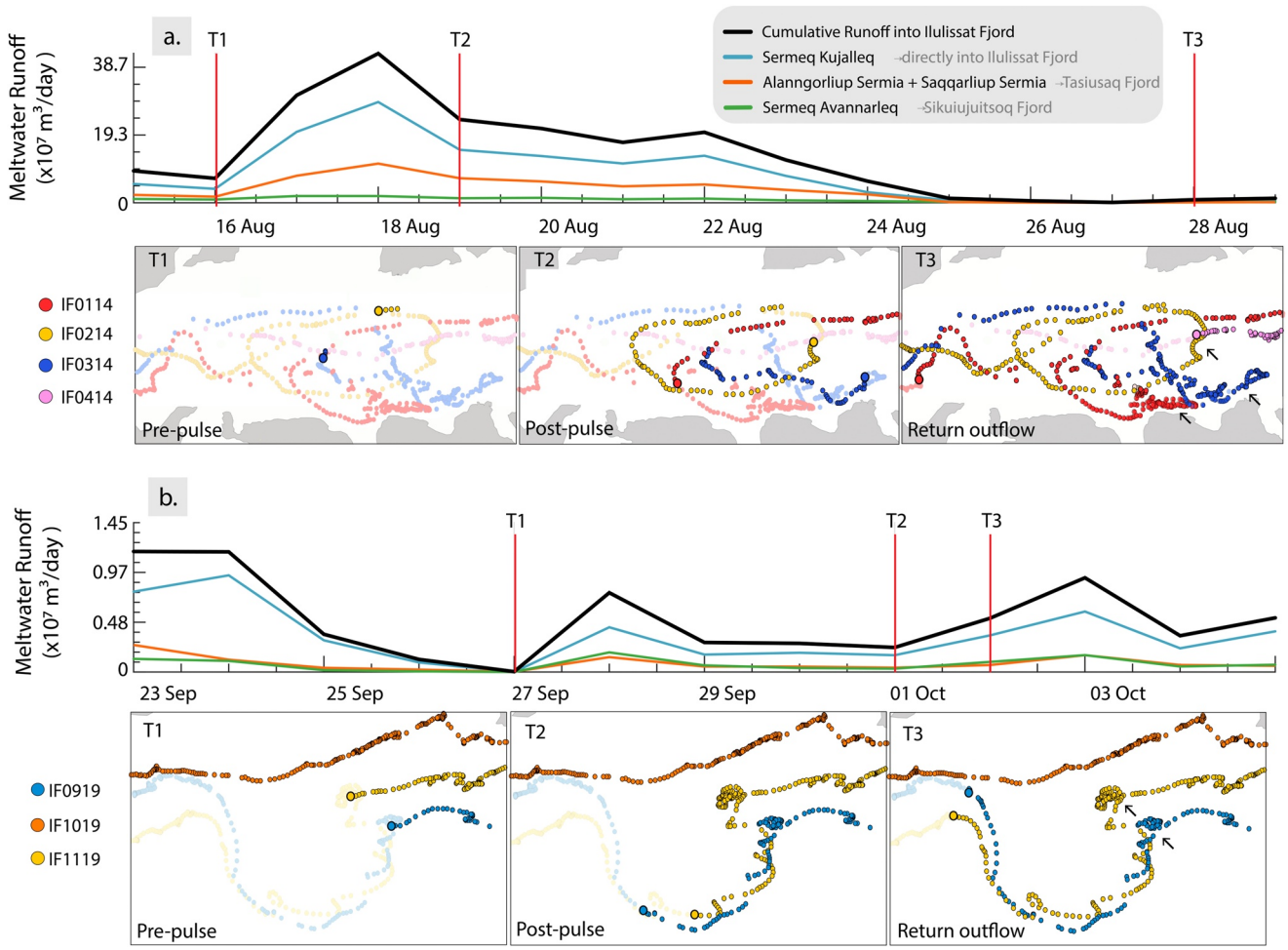

Figure 8. Timing of meltwater runoff pulses in relation to iceberg position in Ilulissat Icefjord. Cumulative meltwater runoff adjusted for transit time to Ilulissat Icefjord (solid black line) in 2014 (a) and 2019 (b) and iceberg position across three different timestamps (red vertical lines); Pre-runoff pulse, post-runoff pulse, and when icebergs return to flow down-fjord. Filled multi-colored circles represent individual GPS-instrumented icebergs, the largest circles representing iceberg position at the corresponding timestamp (T1, T2, and T3). Faded circles represent iceberg trajectory beyond each timestamp, and arrows (T3) note the potential locations of rotationally driven boundary currents.

found strong glacier-mélange linkages and weak to null mélange-ocean current linkages (Amundson et al., 2010; Cassotto et al., 2021). Additionally, modeled outputs suggest that surface currents in a mélange are greatly reduced, and instead of flowing at the surface, the down-fjord flow is located below the drafts of the deepest icebergs (Hughes, 2022). Therefore, due to the tightly packed nature of the mélange and the forced location of the currents, tracking icebergs in the mélange region is not representative of fjord circulation and we exclude the mélange region in analysis of surface circulation.

In the mid-fjord and fjord mouth regions of Ilulissat Icefjord, icebergs are freely floating, and iceberg trajectory, as well as the presence or absence of deviations from that trajectory, coincide with the timing of meltwater delivery, which we propose is the dominant control in these regions. During the instrumental period, icebergs transited past both Sikuiujuitsoq fjord to the north and Tasiusaq fjord to the south in the mid-fjord region, as well as through the fjord mouth region, which is absent of tributary confluences. This dichotomy within the same physical environment, as well as variability in hydrography between years, enables analysis of the impact of increases, decreases, and the absence of runoff-induced circulation on iceberg trajectory. In both 2014 and 2019, icebergs transited through a tributary confluence before, during, and after the arrival of a runoff pulse at that location, enabling comparison of behavior. In the absence of tributary runoff pulses, icebergs moved down-fjord past tributary fjord confluences and through the fjord mouth region without any deviation in speed or direction (Figure 8: IF0414, IF1019). However, during the onset of a runoff pulse, the down-fjord iceberg trajectory was interrupted in the mid-fjord region (Figure 8,

T1–T2) and icebergs either reversed direction up-fjord (2014) or moved away from the tributary fjord confluence sourcing the pulse (2019). In 2014, the onset of a runoff pulse from Tasiusaq Fjord (15 August) coincided with the approach of three icebergs (IF0114, IF0214, IF0314) to the confluence area. At the onset of the runoff pulse (1.2×10^7 m³ d^{-1}, Figure 8a, T1), the three icebergs reversed trajectory over the span of 3 days, transiting back up fjord ~7–10 km, and reaching maximum speeds of ~$2.8–6.7 \times 10^4$ m d^{-1} (Figure 8a, T2). When the pulse decreased in magnitude (+9 days), the icebergs returned to a direct down-fjord trajectory (Figure 8a, T3). In 2019, the onset of a runoff pulse from Sikuiujuitsoq Fjord (27 September 2019, 2.0×10^7 m³ d^{-1}) coincided with the approach of two icebergs (IF0919, IF1110) to the confluence area. In this instance, the runoff pulse was greater in volume than in 2014, but entering a fjord that was overall much slower. In this instance, icebergs transited ~3 km to the opposite side of the fjord (Figure 8b, T2), reaching maximum speeds of ~$1.7–2.6 \times 10^4$ m d^{-1}. After 5 days, the icebergs moved beyond the confluence with Sikuiujuitsoq Fjord and into the confluence with Tasiusaq Fjord, where runoff was again present, and the icebergs transited back north ~3 km before returning to their original trajectory (Figure 8, T3).

While we consider the impact of calving events, glacier velocity, wind, and meltwater runoff in this study, previous work points to potential additional processes that could account for the observed non-linear iceberg behavior in the mid-fjord region. Modeling has shown the possibility of mesoscale eddies in glacial fjords (e.g., Zhao et al., 2023) which are long-lived (~75 days in the mid-fjord region) and spatially distributed along the length of Ilulissat Icefjord. In this study, the iceberg deviations observed in Ilulissat Icefjord were of the same order of magnitude (~10 km in diameter), but isolated to the mid-fjord region, had a lifespan of only a few days, and were overall faster than iceberg velocities observed in the mesoscale eddies (2020 eddies: $1.0–1.25 \times 10^3$ m d^{-1} vs. GPS-instrumented icebergs: $1.7–6.7 \times 10^4$ m d^{-1}). Due to these differences, it is unlikely that mesoscale eddies explain the observed non-linear behavior. Another explanation for the non-uniform response could be due to variability in iceberg size, and therefore degree of contact with individual water masses possessing variable water velocity with depth (e.g., Schild et al., 2021; Sutherland, Roth, et al., 2014). However, when comparing the keel depths, the icebergs that did not deviate from their trajectory (240, 190 m) were comparable in size and to those that did deviate (183–379 m; Table 1), which also eliminates this alternative explanation. Lastly, we evaluated the potential impact of rotation and rotationally driven boundary currents on the non-uniform iceberg behavior (e.g., Zhao et al., 2023). In instances of deviation initiated at the confluence of Sikuiujuitsoq Fjord (five instances across 2014 and 2019), there is a small (<600 m) deflection up-fjord (Figure 8, T3, arrows), before icebergs continue on each larger deviation. This small-scale deflection could suggest the presence of a rotationally driven boundary current, however does not support the observed larger scale non-uniform deviations. We also considered the impact of rotational effects, where the Rossby radius of deformation ranged from 9 to 12 km (measured in Gladish et al., 2015), wider than the width of Ilulissat Icefjord, and could contribute to directional deflections. We found that in all large-scale deviations, icebergs were deflected to the right of the incoming runoff pulse, suggesting that tributary fluxes are behaving similarly to coastal currents upon exiting tributary fjords. However, we do not see this directional deflection in the absence of runoff pulses, and therefore conclude that the influence of rotation is important on iceberg trajectory, but only as much as influencing the deflection direction during periods of increased tributary fjord flux.

6. Conclusion

In this study, we use a combination of glacier, ocean, and atmospheric data sets to identify drivers of freely floating iceberg movement, as a proxy for upper-layer (<250 m) fjord circulation in Ilulissat Icefjord, west Greenland. During the summers of 2014 and 2019, high temporal resolution (hourly) GPS units were deployed via helicopter on a total of 13 icebergs spanning the length of Ilulissat Icefjord. These iceberg position measurements revealed spatial differences in iceberg movement, dependent upon their location within the fjord. These three distinct regions we designated as mélange, mid-fjord, and fjord mouth regions. After accounting for meltwater runoff, wind, calving events, and glacier velocity, we identified two dominant drivers of iceberg movement: glacier behavior (calving, glacier velocity) and meltwater runoff. In the mélange region, iceberg speed and residence time changed in concert with the velocity of Sermeq Kujalleq and short-term accelerations in iceberg position (<4 km, ~1–3 hr) coincided with the timing of calving events. However, there was no discernible change in iceberg position during peaks in meltwater runoff or wind events supporting the conclusion of glacier behavior-dominated iceberg movement in this region, which is consistent with prior findings (e.g., Amundson et al., 2010; Cassotto et al., 2021). In the mid-fjord region, icebergs were freely floating, and their behavior coincided with changes in runoff-induced flux from tributary fjords. During instances where the arrival of runoff

pulses coincided with icebergs transiting through these confluences in Ilulissat Icefjord, icebergs deviated from their down-fjord trajectory, either reversing up-fjord (2014), or across-fjord, away from the arrival location (2019), before returning to their original trajectory upon completion of the runoff pulse. In the absence of runoff pulses, icebergs maintained their down-fjord trajectory, continuing past confluence locations without deviation. In the fjord mouth region, icebergs were again freely floating, and without exposure to runoff pulses, continued in a purely down-fjord trajectory. We considered wind events, mesoscale eddies, rotation, and differing iceberg geometries as potential drivers of non-linear iceberg movement, but all possibilities to account for the non-uniform trajectories were eliminated due to inconsistencies between predicted and observed behavior. Overall, this study provides observational constraints on upper-layer fjord circulation and highlights the importance of tributary fjords on upper-layer fjord circulation. Additionally, this study demonstrates the utility and caveats associated with using natural drifters (icebergs) to infer upper layer circulation. Recent advances in both regional-scale and global climate models have highlighted the influence of icebergs on freshwater injection and ocean modification (Davison et al., 2020; Hager et al., 2022; Kajanto et al., 2022; Zhao et al., 2022), however we should continue to pursue the inclusion of complex geometry, non-linear movement, and the influence of meltwater runoff on fjord circulation in systems thinking and modeling.

Data Availability Statement

Raw 2014 CTD data are available at NOAA National Centers for Environmental Information (NCEI Accession 0162649; https://accession.nodc.noaa.gov/0162649) and accessed on 19 January 2021 (Straneo & Beaird, 2017). The staged on-iceberg GPS positions, SfM iceberg surface point clouds, and 2019 (X)CTD data can be found at Arctic Data Center (https://arcticdata.io/) at https://doi.org/10.18739/A2MS3K33N (Baratta et al., 2023).

Acknowledgments
Field work and data collection was supported by the Advanced Climate Dynamics Courses (ACDC) 2014 summer school, NSF-OPP Award OCE-1536856 (to Fiammetta Straneo), NSF-OPP Award 1552232 (to DAS) and internal University of Oregon support (to DAS). Data processing and analysis was supported by NSF NRT-NNA award 2021713 (for SJNB) and NASA NIP award 80NSSC21K0945 (to KMS, for SJNB). We thank ACDC summer school students for the 2014 CTD collection, and Fiammetta Straneo and Nicholas Beaird for the 2014 on-iceberg GPS deployment. We also thank Mark Carey and Casey Shoop for assisting in the 2019 X-CTD collection and on-iceberg GPS deployment. Additionally, we thank Brice Noël at the Institute for Marine and Atmospheric Research (IMAU) for processing and staging RACMO 2.3p2 results for our study period, as well as the two anonymous reviewers who provided helpful insight and feedback that greatly improved this manuscript.

References

Amundson, J. M., Fahnestock, M., Truffer, M., Brown, J., Lüthi, M. P., & Motyka, R. J. (2010). Ice mélange dynamics and implications for terminus stability, Jakobshavn Isbræ, Greenland. *Journal of Geophysical Research*, *115*(F1), F01005. https://doi.org/10.1029/2009jf001405

Baratta, S., Schild, K. M., & Sutherland, D. (2023). *Ilulissat Icefjord, Greenland iceberg positional data and expendable conductivity-temperature-depth (XCTD), August 2014 and 2019*. NSF Arctic Data Center. https://doi.org/10.18739/A2MS3K33N

Beaird, N., Straneo, F., & Jenkins, W. (2017). Characteristics of meltwater export from Jakobshavn Isbræ and Ilulissat Icefjord. *Annals of Glaciology*, *58*(74), 107–117. https://doi.org/10.1017/aog.2017.19

Cappelen, J. (2021). Denmark—DMI historical climate data collection 17682020.

Carroll, D., Sutherland, D. A., Shroyer, E. L., Nash, J. D., Catania, G. A., & Stearns, L. A. (2015). Modeling turbulent subglacial meltwater plumes: Implications for fjord-scale buoyancy-driven circulation. *Journal of Physical Oceanography*, *45*(8), 2169–2185. https://doi.org/10.1175/jpo-d-15-0033.1

Cassotto, R., Burton, J. C., Amundson, J. M., Fahnestock, M. A., & Truffer, M. (2021). Granular decoherence precedes ice mélange failure and glacier calving at Jakobshavn Isbræ. *Nature Geoscience*, *14*(6), 417–422. https://doi.org/10.1038/s41561-021-00754-9

Cassotto, R., Fahnestock, M., Amundson, J. M., Truffer, M., & Joughin, I. (2015). Seasonal and interannual variations in ice melange and its impact on terminus stability, Jakobshavn Isbræ, Greenland. *Journal of Glaciology*, *61*(225), 76–88. https://doi.org/10.3189/2015JoG13J235

Cenedese, C., & Adduce, C. (2010). A new parameterization for entrainment in overflows. *Journal of Physical Oceanography*, *40*(8), 1835–1850. https://doi.org/10.1175/2010jpo4374.1

Cenedese, C., & Gatto, V. M. (2016). Impact of a localized source of subglacial discharge on the heat flux and submarine melting of a tidewater glacier: A laboratory study. *Journal of Physical Oceanography*, *46*(10), 3155–3163. https://doi.org/10.1175/jpo-d-16-0123.1

Cowton, T., Nienow, P., Sole, A., Wadham, J., Lis, G., Bartholomew, I., et al. (2013). Evolution of drainage system morphology at a land-terminating Greenlandic outlet glacier. *Journal of Geophysical Research: Earth Surface*, *118*(1), 29–41. https://doi.org/10.1029/2012jf002540

Cowton, T., Slater, D., Sole, A., Goldberg, D., & Nienow, P. (2015). Modeling the impact of glacial runoff on fjord circulation and submarine melt rate using a new subgrid-scale parameterization for glacial plumes. *Journal of Geophysical Research: Oceans*, *120*(2), 796–812. https://doi.org/10.1002/2014jc010324

Davison, B. J., Cowton, T. R., Cottier, F. R., & Sole, A. J. (2020). Iceberg melting substantially modifies oceanic heat flux towards a major Greenlandic tidewater glacier. *Nature Communications*, *11*(1), 5983. https://doi.org/10.1038/s41467-020-19805-7

Everett, A., Kohler, J., Sundfjord, A., Kovacs, K. M., Torsvik, T., Pramanik, A., et al. (2018). Subglacial discharge plume behaviour revealed by CTD-instrumented ringed seals. *Scientific Reports*, *8*(1), 13467. https://doi.org/10.1038/s41598-018-31875-8

Farmer, D. M., & Freeland, H. J. (1983). The physical oceanography of fjords. *Progress in Oceanography*, *12*(2), 147–219.

Felikson, D., Bartholomaus, T. C., Catania, G. A., Korsgaard, N. J., Kjær, K. H., Morlighem, M., et al. (2017). Inland thinning on the Greenland ice sheet controlled by outlet glacier geometry. *Nature Geoscience*, *10*(5), 366–369. https://doi.org/10.1038/ngeo2934

Garcia, A. M. P., Geyer, W. R., & Randall, N. (2021). Exchange flows in tributary creeks enhance dispersion by tidal trapping. *Estuaries and Coasts*, *45*(2), 363–381. https://doi.org/10.1007/s12237-021-00969-4

GEBCO. (2020). Bathymetric chart of the Arctic Ocean (IBCAO). https://doi.org/10.5285/a29c5465-b138-234d-e053-6c86abc040b9

Gladish, C. V., Holland, D. M., Rosing-Asvid, A., Behrens, J. W., & Boje, J. (2015). Oceanic boundary conditions for Jakobshavn glacier. Part I: Variability and renewal of Ilulissat Icefjord waters, 2001–14. *Journal of Physical Oceanography*, *45*(1), 3–32. https://doi.org/10.1175/jpo-d-14-0044.1

Gong, W., Chen, L., Zhang, H., Yuan, L., & Chen, Z. (2020). Plume dynamics of a lateral river tributary influenced by river discharge from the estuary head. *Journal of Geophysical Research: Oceans*, *125*(2), e2019JC015580. https://doi.org/10.1029/2019jc015580

Hager, A. O., Sutherland, D. A., Amundson, J. M., Jackson, R. H., Kienholz, C., Motyka, R. J., & Nash, J. D. (2022). Subglacial discharge reflux and buoyancy forcing drive seasonality in a silled glacial fjord. *Journal of Geophysical Research: Oceans*, *127*(5), e2021JC018355. https://doi.org/10.1029/2021jc018355

Holland, D. M., Thomas, R. H., de Young, B., Ribergaard, M. H., & Lyberth, B. (2008). Acceleration of Jakobshavn Isbræ triggered by warm subsurface ocean waters. *Nature Geoscience*, *1*(10), 659–664. https://doi.org/10.1038/ngeo316

Howat, I. (2020). *MEaSUREs Greenland ice velocity: Selected glacier site velocity maps from optical images*. NASA National Snow and Ice Data Center Distributed Active Archive Center. https://doi.org/10.5067/RRFY5IW94X5W

Howat, I., Negrete, A., & Smith, B. (2015). *MEaSUREs Greenland ice mapping project (GIMP) digital elevation model, version 1*. NASA National Snow and Ice Data Center Distributed Active Archive Center. https://doi.org/10.5067/NV34YUIXLP9W

Hughes, K. G. (2022). Pathways, form drag, and turbulence in simulations of an ocean flowing through an ice mélange. *Journal of Geophysical Research: Oceans*, *127*(6), e2021JC018228. https://doi.org/10.1029/2021JC018228

Jenkins, A. (2011). Convection-driven melting near the grounding lines of ice shelves and tidewater glaciers. *Journal of Physical Oceanography*, *41*(12), 2279–2294. https://doi.org/10.1175/jpo-d-11-03.1

Joughin, I., Howat, I. M., Fahnestock, M., Smith, B., Krabill, W., Alley, R. B., et al. (2008). Continued evolution of Jakobshavn Isbrae following its rapid speedup. *Journal of Geophysical Research*, *113*(F4), F04006. https://doi.org/10.1029/2008jf001023

Joughin, I., Shean, D. E., Smith, B. E., & Floricioiu, D. (2020). A decade of variability on Jakobshavn Isbrae: Ocean temperatures pace speed through influence on melange rigidity. *The Cryosphere*, *14*(1), 211–227. https://doi.org/10.5194/tc-14-211-2020

Kajanto, K., Straneo, F., & Nisancioglu, K. (2022). Impact of icebergs on the seasonal submarine melt of Sermeq Kujalleq. *The Cryosphere*. https://doi.org/10.5194/tc-2022-136

Khazendar, A., Fenty, I. G., Carroll, D., Gardner, A., Lee, C. M., Fukumori, I., et al. (2019). Interruption of two decades of Jakobshavn Isbrae acceleration and thinning as regional ocean cools. *Nature Geoscience*, *12*(4), 277–283. https://doi.org/10.1038/s41561-019-0329-3

Klinck, J. M., O'Brien, J. J., & Svendsen, H. (1981). A simple model of fjord and coastal. *Journal of Physical Oceanography*, *11*(12), 1612–1626. https://doi.org/10.1175/1520-0485(1981)011<1612:asmofa>2.0.co;2

Lindbäck, K., Kohler, J., Pettersson, R., Nuth, C., Langley, K., Messerli, A., et al. (2018). Subglacial topography, ice thickness, and bathymetry of Kongsfjorden, northwestern Svalbard. *Earth System Science Data*, *10*(4), 1769–1781. https://doi.org/10.5194/essd-10-1769-2018

Moon, T., & Joughin, I. (2008). Changes in ice front position on Greenland's outlet glaciers from 1992 to 2007. *Journal of Geophysical Research*, *113*(F2), F02022. https://doi.org/10.1029/2007jf000927

Morlighem, M., Williams, C. N., Rignot, E., An, L., Arndt, J. E., Bamber, J. L., et al. (2017). BedMachine v3: Complete bed topography and ocean bathymetry mapping of Greenland from multibeam echo sounding combined with mass conservation. *Geophysical Research Letters*, *44*(21), 11051–11061. https://doi.org/10.1002/2017GL074954

Motyka, R. J., Hunter, L., Echelmeyer, K. A., & Connor, C. (2003). Submarine melting at the terminus of a temperate tidewater glacier, LeConte Glacier, Alaska, U.S.A. *Annals of Glaciology*, *36*, 57–65. https://doi.org/10.3189/172756403781816374

Motyka, R. J., Truffer, M., Fahnestock, M., Mortensen, J., Rysgaard, S., & Howat, I. (2011). Submarine melting of the 1985 Jakobshavn Isbrae floating tongue and the triggering of the current retreat. *Journal of Geophysical Research*, *116*(F1), F01007. https://doi.org/10.1029/2009jf001632

Mouginot, J., Rignot, E., Bjork, A. A., van den Broeke, M., Millan, R., Morlighem, M., et al. (2019). Forty-six years of Greenland Ice Sheet mass balance from 1972 to 2018. *Proceedings of the National Academy of Sciences of the United States of America*, *116*(19), 9239–9244. https://doi.org/10.1073/pnas.1904242116

Noël, B., van de Berg, W. J., Machguth, H., Lhermitte, S., Howat, I., Fettweis, X., & van den Broeke, M. R. (2016). A daily, 1 km resolution data set of downscaled Greenland ice sheet surface mass balance (1958–2015). *The Cryosphere*, *10*(5), 2361–2377. https://doi.org/10.5194/tc-10-2361-2016

O'Leary, M., & Christoffersen, P. (2013). Calving on tidewater glaciers amplified by submarine frontal melting. *The Cryosphere*, *7*(1), 119–128. https://doi.org/10.5194/tc-7-119-2013

Rennermalm, A. K., Smith, L. C., Chu, V. W., Box, J. E., Forster, R. R., Van den Broeke, M. R., et al. (2013). Evidence of meltwater retention within the Greenland ice sheet. *The Cryosphere*, *7*(5), 1433–1445. https://doi.org/10.5194/tc-7-1433-2013

Salcedo-Castro, J., Bourgault, D., & de Young, B. (2011). Circulation induced by subglacial discharge in glacial fjords: Results from idealized numerical simulations. *Continental Shelf Research*, *31*(13), 1396–1406. https://doi.org/10.1016/j.csr.2011.06.002

Sanchez, R., Slater, D., & Straneo, F. (2023). Delayed freshwater export from a Greenland tidewater glacial fjord. *Journal of Physical Oceanography*, *53*(5), 1291–1309. https://doi.org/10.1175/JPO-D-22-0137.1

Schild, K. M., & Hamilton, G. S. (2013). Seasonal variations of outlet glacier terminus position in Greenland. *Journal of Glaciology*, *59*(216), 759–770. https://doi.org/10.3189/2013JoG12J238

Schild, K. M., Renshaw, C. E., Benn, D. I., Luckman, A., Hawley, R. L., How, P., et al. (2018). Glacier calving rates due to subglacial discharge, fjord circulation, and free convection. *Journal of Geophysical Research: Earth Surface*, *123*(9), 2189–2204. https://doi.org/10.1029/2017jf004520

Schild, K. M., Sutherland, D. A., Elosegui, P., & Duncan, D. (2021). Measurements of iceberg melt rates using high-resolution GPS and iceberg surface scans. *Geophysical Research Letters*, *48*(3), e2020GL089765. https://doi.org/10.1029/2020gl089765

Slater, D. A., & Straneo, F. (2022). Submarine melting of glaciers in Greenland amplified by atmospheric warming. *Nature Geoscience*, *15*(10), 794–799. https://doi.org/10.1038/s41561-022-01035-9

Slater, D. A., Straneo, F., Das, S. B., Richards, C. G., Wagner, T. J. W., & Nienow, P. W. (2018). Localized plumes drive front-wide ocean melting of a Greenlandic tidewater glacier. *Geophysical Research Letters*, *45*(22), 12350–12358. https://doi.org/10.1029/2018gl080763

Smith, B., Fricker, H. A., Gardner, A. S., Medley, B., Nilsson, J., Paolo, F. S., et al. (2020). Pervasive ice sheet mass loss reflects competing ocean and atmosphere processes. *Science*, *368*(6496), 1239–1242. https://doi.org/10.1126/science.aaz5845

Stigebrandt, A. (2012). Hydrodynamics and Circulation of Fjords. In L. Bengtsson, R. W. Herschy, & R. W. Fairbridge (Eds.), *Encyclopedia of lakes and reservoirs* (pp. 327–344). Springer Netherlands. https://doi.org/10.1007/978-1-4020-4410-6_247

Straneo, F., & Beaird, N. (2017). TEMPERATURE and SALINITY profiles collected from RV Porsild in Ata Sund, West Greenland from 2014-08-16 to 2014-09-01 (NCEI Accession 0162649) [Dataset]. NOAA National Centers for Environmental Information. https://www.ncei.noaa.gov/archive/accession/0162649

Straneo, F., Curry, R. G., Sutherland, D. A., Hamilton, G. S., Cenedese, C., Våge, K., & Stearns, L. A. (2011). Impact of fjord dynamics and glacial runoff on the circulation near Helheim Glacier. *Nature Geoscience*, *4*(5), 322–327. https://doi.org/10.1038/ngeo1109

Straneo, F., Hamilton, G. S., Sutherland, D. A., Stearns, L. A., Davidson, F., Hammill, M. O., et al. (2010). Rapid circulation of warm subtropical waters in a major glacial fjord in East Greenland. *Nature Geoscience*, *3*(3), 182–186. https://doi.org/10.1038/ngeo764

Sutherland, D. A., Roth, G. E., Hamilton, G. S., Mernild, S. H., Stearns, L. A., & Straneo, F. (2014). Quantifying flow regimes in a Greenland glacial fjord using iceberg drifters. *Geophysical Research Letters*, *41*(23), 8411–8420. https://doi.org/10.1002/2014gl062256

Sutherland, D. A., & Straneo, F. (2012). Estimating ocean heat transports and submarine melt rates in Sermilik Fjord, Greenland, using lowered acoustic Doppler current profiler (LADCP) velocity profiles. *Annals of Glaciology*, *53*(60), 50–58. https://doi.org/10.3189/2012AoG60A050

Sutherland, D. A., Straneo, F., & Pickart, R. S. (2014). Characteristics and dynamics of two major Greenland glacial fjords. *Journal of Geophysical Research: Oceans*, *119*(6), 3767–3791. https://doi.org/10.1002/2013jc009786

Wagner, T. J. W., Dell, R. W., & Eisenman, I. (2017). An analytical model of iceberg drift. *Journal of Physical Oceanography*, *47*(7), 1605–1616. https://doi.org/10.1175/jpo-d-16-0262.1

Wood, M., Rignot, E., Fenty, I., An, L., Bjørk, A., van den Broeke, M., et al. (2021). Ocean forcing drives glacier retreat in Greenland. *Science Advances*, *7*(1), eaba7282. https://doi.org/10.1126/sciadv.aba7282

Xu, Y., Rignot, E., Fenty, I., Menemenlis, D., & Flexas, M. M. (2013). Subaqueous melting of Store Glacier, west Greenland from three-dimensional, high-resolution numerical modeling and ocean observations. *Geophysical Research Letters*, *40*(17), 4648–4653. https://doi.org/10.1002/grl.50825

Zhao, K. X., Stewart, A. L., & McWilliams, J. C. (2021). Geometric constraints on glacial fjord-shelf exchange. *Journal of Physical Oceanography*, *51*(4), 1223–1246. https://doi.org/10.1175/jpo-d-20-00

Zhao, K. X., Stewart, A. L., & McWilliams, J. C. (2022). Linking overturning, recirculation, and melt in glacial fjords. https://doi.org/10.1029/2021GL095706

Zhao, K. X., Stewart, A. L., McWilliams, J. C., Fenty, I. G., & Rignot, E. J. (2023). Standing eddies in glacial fjords and their role in fjord circulation and melt. *Journal of Physical Oceanography*, *53*(3), 821–840. https://doi.org/10.1175/JPO-D-22-0085.1